Article

Cell Reports

Directional R-Loop Formation by the CRISPR-Cas Surveillance Complex Cascade Provides Efficient Off-Target Site Rejection

Graphical Abstract

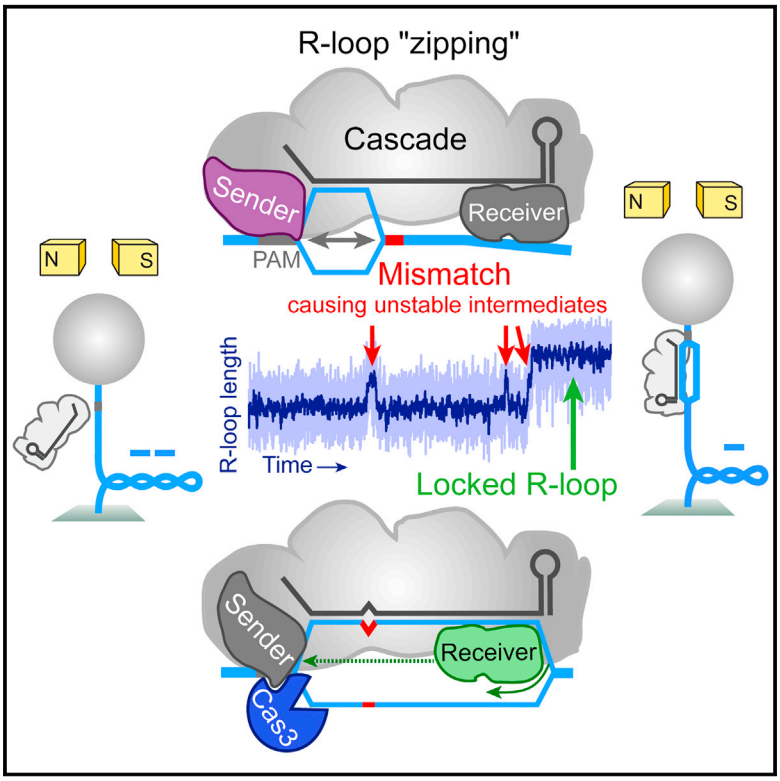

Highlights

- R-loop progression is monitored with close to base-pair resolution
- Target recognition occurs exclusively through a directional R-loop-zipping process
- Intermediate R-loops stall at mutations and collapse in a length-dependent manner
- R-loop locking at protospacer end licenses DNA cleavage without further proofreading

Authors

Marius Rutkauskas, Tomas Sinkunas, ..., Virginijus Siksnys, Ralf Seidel

Correspondence

siksnys@ibt.lt (V.S.), ralf.seidel@uni-muenster.de (R.S.)

In Brief

The CRISPR-Cas surveillance complex Cascade targets invading DNA for destruction with the help of a short crRNA. Rutkauskas et al. use real-time supercoiling experiments on single DNA molecules to directly reveal the impact of mismatches during the directional zipping of the crRNA on a DNA target.

Rutkauskas et al., 2015, Cell Reports *10*, 1534–1543
March 10, 2015 ©2015 The Authors
http://dx.doi.org/10.1016/j.celrep.2015.01.067

CellPress

OPEN ACCESS
CellPress

Cell Reports
Article

Directional R-Loop Formation by the CRISPR-Cas Surveillance Complex Cascade Provides Efficient Off-Target Site Rejection

Marius Rutkauskas,[1] Tomas Sinkunas,[2] Inga Songailiene,[2] Maria S. Tikhomirova,[1] Virginijus Siksnys,[2,*] and Ralf Seidel[1,*]
[1]Institute for Molecular Cell Biology, Westfälische Wilhelms-Universität Münster, 48149 Münster, Germany
[2]Institute of Biotechnology, Vilnius University, Graiciuno 8, Vilnius 02241, Lithuania
*Correspondence: siksnys@ibt.lt (V.S.), ralf.seidel@uni-muenster.de (R.S.)
http://dx.doi.org/10.1016/j.celrep.2015.01.067
This is an open access article under the CC BY-NC-ND license (http://creativecommons.org/licenses/by-nc-nd/3.0/).

SUMMARY

CRISPR-Cas systems provide bacteria and archaea with adaptive immunity against foreign nucleic acids. In type I CRISPR-Cas systems, invading DNA is detected by a large ribonucleoprotein surveillance complex called Cascade. The crRNA component of Cascade is used to recognize target sites in foreign DNA (protospacers) by formation of an R-loop driven by base-pairing complementarity. Using single-molecule supercoiling experiments with near base-pair resolution, we probe here the mechanism of R-loop formation and detect short-lived R-loop intermediates on off-target sites bearing single mismatches. We show that R-loops propagate directionally starting from the protospacer-adjacent motif (PAM). Upon reaching a mismatch, R-loop propagation stalls and collapses in a length-dependent manner. This unambiguously demonstrates that directional zipping of the R-loop accomplishes efficient target recognition by rapidly rejecting binding to off-target sites with PAM-proximal mutations. R-loops that reach the protospacer end become locked to license DNA degradation by the auxiliary Cas3 nuclease/helicase without further target verification.

INTRODUCTION

CRISPR (clustered regularly interspaced short palindromic repeats)-Cas (CRISPR-associated) systems provide bacteria and archaea with RNA-based adaptable immunity against invasion by bacteriophages and plasmids (Barrangou et al., 2007). The CRISPR array comprises conserved repeat sequences interspersed by variable spacer sequences that originate from foreign DNA. Following transcription and subsequent cleavage of the pre-crRNA within the repeats, short crRNAs are produced, each carrying a single spacer (Brouns et al., 2008; Carte et al., 2008). crRNAs together with Cas proteins are then combined into effector complexes that are multimeric for type I and III CRISPR-Cas systems (Brouns et al., 2008; Sinkunas et al., 2013; Zhang et al., 2012; Tamulaitis et al., 2014) or monomeric for type II systems (Gasiunas et al., 2012). Type I and II effector complexes recognize putative DNA targets by establishing base-specific pairing between the crRNA guide and the target sequence (called the "protospacer"), forming a so-called R-loop where the crRNA forms a heteroduplex with the complementary DNA strand while the non-targeting strand is displaced. Importantly, crRNA-guided DNA interference by the type I and II effector complexes requires an additional protospacer-adjacent motif (PAM) located in the vicinity of the target. The PAM sequence, which is absent in the CRISPR array but present in the invading DNA, is important for the discrimination between "self" and "non-self" (Deveau et al., 2008). Mismatches between the crRNA and the protospacer "seed" sequence adjacent to the PAM typically abolish interference, whereas mismatches in the PAM-distal sequence are less inhibitive (Semenova et al., 2011; Fineran et al., 2014). Tolerance of mismatches reduces the possibility that invaders could escape CRISPR immunity due to mutational drift in protospacer sequences and is thus beneficial for the host. Contrarily, a low tolerance of target mismatches is desired in genome-engineering applications that recently emerged using the Cas9 effector complex of type II systems (Mali et al., 2013). Although high-resolution structures of type I and II effector complexes with and without bound single-stranded target DNA recently became available (Mulepati et al., 2014; Jackson et al., 2014; Zhao et al., 2014; Anders et al., 2014), the mechanism by which R-loop formation allows discrimination between correct (on-target) and incorrect (off-target) sites remains to be resolved.

Based on the analysis of the phage escape mutants, Semenova et al. (2011) proposed a directional model for target discrimination by *E. coli* Cascade. According to this model, the crRNA "seed" sequence plays a key role in the initial scanning for a matching sequence, before base pairing over the entire protospacer occurs to form a stable R-loop. In addition to phage escape, also biochemical parameters, such as the lifetime of Cas9 on target DNA (Sternberg et al., 2014) or the stability of R-loops formed by Cascade (Szczelkun et al., 2014), appeared to be affected by the position of protospacer mutations. These observations further supported a directional R-loop formation. However, we note that they can still not rule out a direction-independent R-loop formation, where target discrimination relies on overall thermal equilibrium (rather than the first mutation

encountered). In this case, a mismatch-sensitive position bias would result instead from specific constraints imposed by the locally positioned proteins.

Here, we provide a stringent test for unidirectional R-loop formation by systematically analyzing the effect of mismatches in the protospacer sequence for a *Streptococcus thermophilus* (*St*) Cascade effector complex. Applying single-molecule supercoiling experiments (Brutzer et al., 2010; Szczelkun et al., 2014), we are able to directly observe the formation of full R-loops and, most critically, the stalling of unstable R-loop intermediates in front of mismatches. The unstable R-loops map to the region between the PAM and the mismatch as predicted for unidirectional R-loop zipping and have a length-dependent stability, resulting in rapid rejection of targets with PAM-proximal mutations. Once the R-loop propagates across the complete protospacer, it becomes locked (i.e., highly stable). This triggers rapid DNA cleavage through recruitment of the Cas3 helicase/nuclease without further protospacer verification, even in presence of "seed" mutations. Thus, the dynamic and directional R-loop-zipping process provides the only selection of cleavage targets. Target recognition is therefore the result of a kinetic readout and not of the total base-pairing thermodynamics per se. Our dissection of the R-loop formation process provides an important basis for quantitatively predicting on-target- and off-target-binding efficiencies of CRISPR-Cas systems with important implication for their application in genome engineering.

RESULTS

Detection of Single Cascade-Induced R-Loops

In *St*-Cascade, the Cas proteins, plus a 61-nt crRNA assemble with the stoichiometry $Cse1_1Cse2_2Cas7_6Cas5_1Cas6e_1crRNA_1$, forming an ~400 kDa ribonucleoprotein complex (Sinkunas et al., 2013). The crRNA contains a 33-nt spacer sequence that is flanked by 5′ and 3′ handles. A dinucleotide AA PAM in the target DNA is also required for successful R-loop formation. DNA degradation is carried out by the separate Cas3 helicase-nuclease that is recruited to the R-loop-effector complex (Sinkunas et al., 2011, 2013; Westra et al., 2012; Mulepati and Bailey, 2013).

To monitor the formation of Cascade-induced R-loops, we used a previously developed magnetic-tweezers-based DNA supercoiling assay (Szczelkun et al., 2014). We attached a magnetic bead to one end of a single 2.1-kbp DNA molecule containing a PAM and a single protospacer (Figure 1A) and tethered the other DNA end to the bottom of a fluidic cell. A pair of magnets placed above the cell was used to stretch the DNA and to supercoil it by rotating the magnets. Simultaneously, we measured the DNA length from the magnetic bead *z*-position using video microscopy (Otto et al., 2010; Huhle et al., 2015). DNA supercoiling at constant force results in a characteristic bell-shaped DNA length-versus-turn curve (gray curve in Figure 1B). Initially, the DNA length stays constant. Once sufficient twist is generated, the DNA length decreases with the applied turns due to the formation of a plectonemic superhelix (Mosconi et al., 2009; Kauert et al., 2011; Forth et al., 2008; Oberstrass et al., 2012). Upon R-loop formation by Cascade, the DNA target is unwound over 33 bp, which adds approximately three turns of positive supercoiling to the adjacent DNA. Such a change in supercoiling can be readily detected as a shift of the whole supercoiling curve or as a DNA length change at a fixed number of introduced turns (Howan et al., 2012; Szczelkun et al., 2014; Figure 1B).

R-loop formation on a substrate containing a matching (WT) protospacer and a consensus AA dinucleotide PAM is directly seen as a discrete DNA length change at low negative supercoiling and low force (Figure 1C, green arrow). Under these conditions, the DNA is still almost fully extended (stable plectonemes have yet to form) and the mechanical torque in the DNA corresponds to ~−2 pN nm. Upon rotation of the magnets to produce positive supercoiling, the formation of a stable R-loop is indicated by a stable shift of the supercoiling curve toward lower turns (green compared to gray curve in Figure 1C). The R-loop dissociated only when the force was increased to produce a torque of ~+20 pN nm. Dissociation was seen as a sudden DNA length change (red curve in Figure 1C). Further Cascade-induced R-loop formation-dissociation events could then be induced by cycling between the low negative torque and high positive torque regimes. As shown before (Szczelkun et al., 2014), this provides quantitative information about the torque-assisted kinetics of R-loop formation/dissociation, the R-loop length (determined from the shift of the supercoiling curve), and the R-loop stability (determined from the dissociation torque).

R-Loop Formation and Dissociation on Target Sites with Single Mutations

We applied the assay described above to monitor R-loop formation on protospacers bearing single point mutations of the WT target. This included mutations in the seed region at positions 2, 4, and 8 as well as in the remaining protospacer sequence at positions 15, 18, 19, 20, and 22 (Figure 1A; substrates called M2, M4, etc.). For all of the mutants, we carried out extensive supercoiling cycle experiments at 9 nM Cascade and analyzed the mean R-loop formation and dissociation times as function of torque. A representative supercoiling cycle (Figure 1D) is shown for the M2 substrate that required much more negative supercoiling (~4-fold increased torque) for R-loop formation compared to the WT target, whereas R-loop dissociation conditions were similar to the WT protospacer. For all mutants, greater negative torque accelerated R-loop formation, whereas greater positive torque accelerated R-loop dissociation (Figure 2A). For seed mutations, R-loop formation was slowest and required the highest assisting negative torques (Figure 2A, left), in agreement with the finding that these mutations allow phage escape (Semenova et al., 2011). This effect was most pronounced for M2 and M4. With the exception of M19, R-loop formation for protospacer mutants outside the seed region also required higher negative torque values compared to WT (or longer wait times when extrapolated to comparable torque values). In contrast, the dissociation times were not significantly affected (Figure 2A).

Supercoiling Changes Reveal Intermediate R-Loops between PAM and Mismatch

To gain further insight into the inhibitory effect of protospacer mutations, we analyzed the supercoiling changes associated

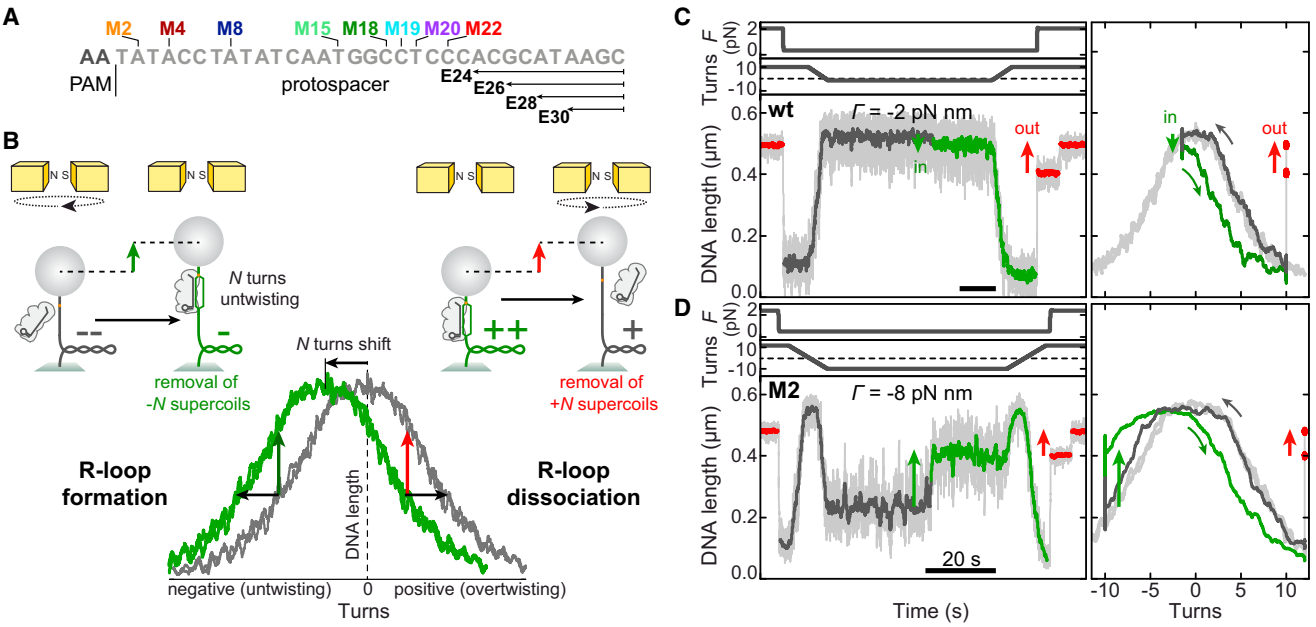

Figure 1. Detection of Single-Cascade-Induced R-Loops on a Matching and a Mismatched Protospacer

(A) Sequence of the non-target strand used in the experiments with mutated positions indicated. Single point mutations were labeled with M; mutations over a whole stretch at the protospacer end with E.

(B) Principle of R-loop detection through single-molecule supercoiling. DNA molecules attached to magnetic beads are supercoiled by magnet rotation. R-loop formation causes local DNA unwinding and thus overwinding of the adjacent DNA. The characteristic plot of DNA length versus introduced turns in absence of an R-loop (gray curve) is shifted to the left by the number of helical turns being untwisted by the R-loop (green curve). When holding the DNA at constant negative supercoiling (assisting R-loop formation), R-loop formation is seen as a DNA length change (green arrow). Correspondingly, R-loop dissociation is seen at positive supercoiling as a similar length change (red arrow).

(C) R-loop formation-dissociation cycle for the WT protospacer. On a DNA held at 0.3 pN, −1.5 turns were introduced (gray curve part), providing the indicated torque Γ. After a delay, R-loop formation is seen as an abrupt length decrease (green vertical arrow, transition from gray to green line). Subsequently, positive supercoiling was applied (green curve part) and the force raised (onset of red curve part) to generate high positive torque. R-loop dissociation is seen as an abrupt length increase (red vertical arrow). The left panel shows the DNA length as a time trajectory, whereas the right panel shows it as a function of the applied turns. In the right panel, light gray indicates the supercoiling curve in absence of Cascade, whereas curved arrows indicate the rotation direction.

(D) R-loop formation-dissociation cycle for the M2 protospacer (labeling as in C). R-loop formation occurred at 0.5 pN, −10 turns. An elevated negative torque was required to achieve R-loop formation, hence causing the DNA length to increase.

with R-loop formation (Figure 2B, left). We evaluated the shift of both the left and the right side of the supercoiling curve (i.e., at negative and positive supercoiling, respectively; see arrows in inset of Figure 2B, left). We selected supercoiling curves where abrupt R-loop formation events were not observed when introducing negative supercoils (dark gray curve in inset of Figure 2B, left). After waiting sufficient time at negative supercoiling to allow R-loop formation, we returned to positive supercoiling (green curve in inset of Figure 2B, left) and determined the shift between the outward and return curves. For the right (positive) side of the supercoiling curves, we obtained a constant shift of 2.7 ± 0.1 turns for all of the mutants and the WT. Similar shifts of 2.7 ± 0.1 turns were also obtained upon R-loop dissociation (Figure 2B, right). The sub-step that occurs during dissociation at high positive torque (Szczelkun et al., 2014) was also independent of the mutation position, with the exception of M18, for which the sub-step was never observed. In contrast, shifts of the left (negative) side of the supercoiling curves seemed to be highly dependent on the mutation position (Figure 2B, left). Whereas the seed mutants M2 and M4 provided shifts of 2.8 ± 0.1 and 2.8 ± 0.2 turns, respectively, the shift for the other mutants (with the exception of M19) decreased linearly with the distance of the mutation from the PAM.

For M19, the left side of the curves did not display any difference, though the shift on the right curve side indicated full R-loop formation (Figure S1) and R-loop dissociation events were always observed upon inducing high positive torque. This behavior is very similar to events with the WT protospacer where R-loop formation occurs at very low negative turns, where the DNA has yet to start forming plectonemes and is still in the extended conformation (Figures 1C and S1). This indicates that M19 does not display any inhibitory effect on the R-loop formation. We therefore attribute M19 to a position where bases are flipped out in the crRNA-DNA hybrid as seen in the *E.coli* Cascade structure (Mulepati et al., 2014). For *E. coli* Cascade, such base flips occur at positions 6, 12, 18, 24, and 30. The +1-nt position shift for the base flips in *St*-Cascade is presumably due to a different assignment of PAM and protospacer, in which the first bp of the *St*-Cascade protospacer is considered as a PAM base pair in the *E.coli* protospacer, whereas the

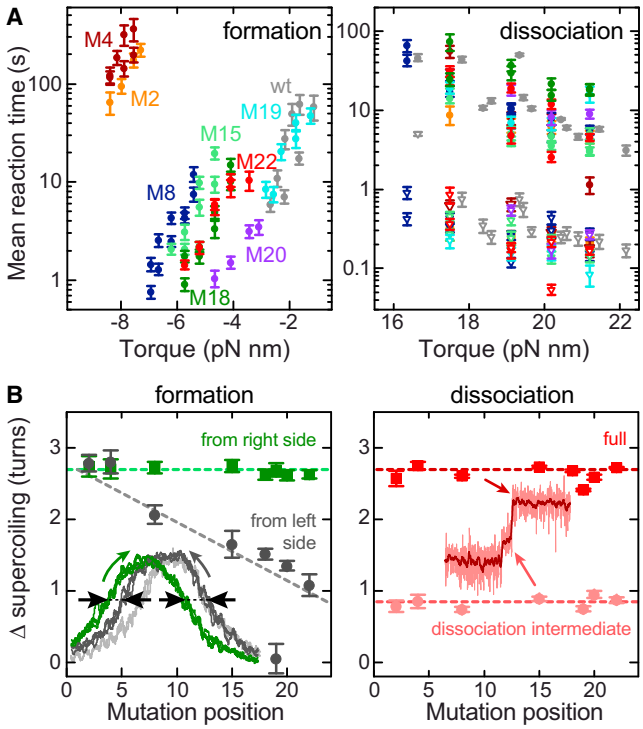

Figure 2. Quantification of R-Loop Formation and Dissociation on Targets with Single Mismatches

(A) Mean times for R-loop formation (left) and dissociation (right) as function of torque for protospacers containing single mismatches at 9 nM Cascade. Increasing negative torque assists faster R-loop formation. R-loop formation is most severely inhibited using mismatches in the seed region (M2, M4, and, to a lower extent, M8) such that much-higher torque is required to achieve R-loop formation in the 10–100 s range. Mismatches M15, M18, and M22 outside the seed region also inhibit R-loop formation, whereas M19 and M20 behave similar as the WT protospacer. For WT and M19 protospacers, the torque was corrected as described in the Supplemental Information. In contrast to the large differences for R-loop formation, the dissociation times are very similar for all mutants tested. Filled and open symbols represent the time to undergo the first and the second dissociation sub-steps, respectively (see inset in B, right side). Coloring is according to DNA used.

(B) (Left) Supercoiling changes occurring during R-loop formation. The inset shows an R-loop formation experiment for M15 (according to Figure 1D, with the light gray curve being taken in absence of Cascade; see Figure S1 for data of other mismatch positions). The shift of the rotation curve in the presence of Cascade from the initially R-loop free state (dark gray curve in inset) to the R-loop bound state (green curve in inset) is analyzed at negative and positive turns (see black arrows). The green dashed line represents the supercoiling shift at positive turns for the matching protospacer, and the gray dashed line the expected shift that occurs from an R-loop intermediate at the mutation position to the fully formed R-loop. (Right) Supercoiling changes during R-loop dissociation for the full R-loop (red) and for the intermediate (light red). The inset shows an enlarged view of the dissociation event of Figure 1C (red curve part) to reveal the intermediate step during dissociation. All error bars correspond to SEM.

combined length of PAM and protospacer is 35 bp for both systems (Sinkunas et al., 2013). Therefore, protein-induced base flips in the crRNA-DNA hybrid for *St*-Cascade are in fact expected at positions 7, 13, 19, 25, and 31, in agreement with our observation for the M19 protospacer.

Rapid R-loop formation at low negative turns for the WT and the M19 protospacers strongly suggests that the reduced shift of the left part of the supercoiling curve for M8, M15, M18, M20, and M22 (Figure 2B, left) is due to the formation of an intermediate R-loop at low negative turns. This R-loop would be stalled at the mismatch position. The observed shift following incubation at elevated supercoiling would correspond to the final transition from the intermediate to the full R-loop (see Figure S1 for details). If R-loop formation is directional initiating from the PAM and the intermediate stalls at the mismatch, we would predict that the supercoiling change accompanying formation of the R-loop intermediate would increase linearly with the PAM mismatch distance. Consequently, the observed final transition from the intermediate to the R-loop would linearly decrease with the PAM mismatch distance. The experimentally observed shifts agree with this prediction (gray dashed line in Figure 2B, left), providing strong evidence for R-loops that originate from the PAM and directionally expand toward the protospacer end.

Dynamics of Intermediate R-Loops Stalled at Mutation Positions

The above experiments were performed using 9 nM Cascade. To monitor the formation and the dynamics of the intermediate R-loops, we carried out additional experiments at 0.1 nM Cascade. Under these conditions, the R-loop-formation kinetics appeared to be limited by Cascade binding to the DNA. This provided sufficient time for the DNA to be shortened through negative supercoiling before Cascade binding, such that the subsequent dynamic R-loop-formation events were directly observable as a length increase (similar to M2; see Figure 1D). For M8 and M19, R-loop formation always occurred as a single step with a corresponding size of ~2.7 turns, as expected for a full R-loop (Figure 3A). However, for M15, M18, M20, and M22, R-loop intermediates were observed, either as transient short-lived species or as sub-steps on the way to full R-loop formation (Figure 3A). For each mutant, the supercoiling changes associated with the intermediates had a well-defined magnitude, which scaled with the distance between the PAM and mismatch (Figure 3B). For M15 and M18, the intermediate R-loops appeared to be highly dynamic (Figure 3A). They often disappeared without overcoming the mutation, such that full R-loop formation proceeded through multiple cycles of intermediate formation and collapse. Contrarily, for M20 and M22, full R-loops formed typically at once after the intermediate state was occupied for the first time. The probability of spontaneous R-loop collapse was torque dependent and decreased in the order M15 > M18 > M20 > M22 (Figure 3C), suggesting that shorter R-loops are less stable and collapse more rapidly. The fact that we could detect intermediate R-loop formation for M8 at high Cascade concentration, but not at low, indicates that the lifetime of the 7-bp R-loop intermediate is too short to be resolved in our assay as a single event.

The length-dependent collapse of R-loop intermediates will speed up the search for matching targets because initiation of R-loop formation at off-target sites will be rapidly curtailed once a mutation near the PAM is reached. To further substantiate this idea and gain insight into the behavior of the seed mutants, we carried out a competitive electrophoretic mobility shift assay (EMSA) with a labeled WT protospacer and increasing amounts

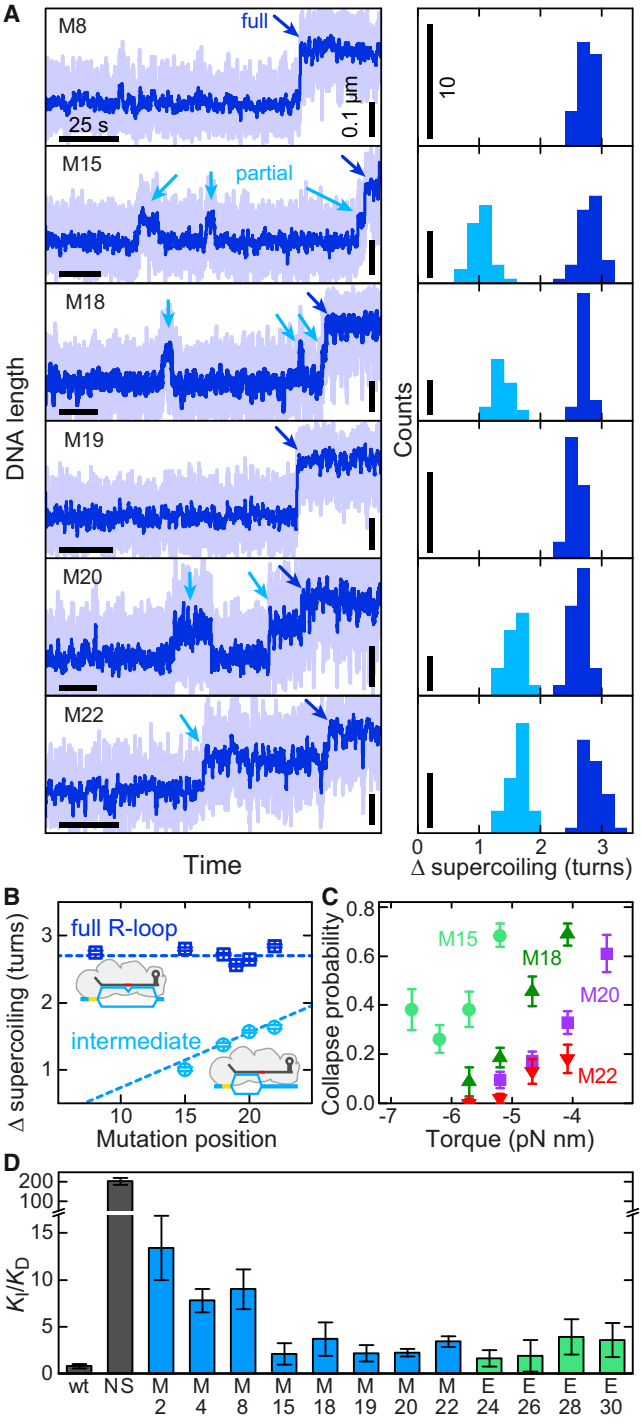

Figure 3. Real-Time Observation of Dynamic R-Loop Intermediates at Mismatch Positions

(A) (Left) Example R-loop formation trajectories at negative supercoiling for protospacers with single mismatches from position 8 onward. During the R-loop formation, constant forces of 0.3, 0.4, 0.25, 0.2, 0.15, and 0.15 pN (from top to bottom) were applied. Blue arrows mark the formation of the full R-loop and light blue arrows the occurrence of intermediate R-loops. The vertical scale bar corresponds to 100 nm. (Right) Histograms for the different mismatch targets of the supercoiling changes associated with full R-loop formation (blue bars) and intermediate R-loop formation (light blue bars). Data were obtained by fitting the length changes associated with R-loop formation in the time trajectories as shown on the left. The vertical scale bar corresponds to ten counts.

(B) Mean supercoiling changes associated with full (blue) and intermediate R-loop formation (light blue) as determined from the histograms in (A). The blue dashed line indicates the supercoiling change for the matching protospacer and the light blue dashed line the expectation for an intermediate R-loop that extends from the PAM to the mismatch position.

(C) Probability that an intermediated R-loop collapses (i.e., that it does not overcome the mutation) as a function of applied torque for the mismatch targets that exhibited intermediate R-loops. Error bars in (B) and (C) correspond to SEM.

(D) Ratio K_I/K_D between the dissociation constants of Cascade binding to the indicated competitor and the WT protospacer as judged from a competitive EMSA assay. NS indicates a non-specific protospacer. Error bars are the SDs from average values from at least three repeat experiments. See also Figure S2.

of unlabeled competitor protospacers bearing mutations (Figure S2). As expected, a non-specific protospacer was found to be the poorest inhibitor of WT DNA binding. Protospacer mutants M2, M4, and M8 were much poorer competitors than protospacers with mutations located further downstream (Figure 3D). We also investigated protospacers for which multiple positions were mutated at the PAM-distal end (called E24, E26, E28, and E30 according to the position of the first mutation; see Figure 1A). Similar results were obtained as for protospacers with non-seed point mutations, despite the fact that R-loop locking is abolished for E24, E26, and E28 (Szczelkun et al., 2014). This confirms that the inhibition is not primarily due to Cascade depletion by formation of locked complexes on competitor substrates but rather due to the formation of intermediate R-loops. Though the competitive EMSA experiments did not reveal systematic differences between the non-seed mutants, they clearly supported the highly transient nature of R-loop intermediates at seed mutations consistent with the single-molecule observations.

R-Loop Locking Triggers DNA Cleavage, Regardless of Seed Mutations

Once a sufficiently long R-loop forms, Cas3-mediated cleavage is initiated (Szczelkun et al., 2014). We next tested whether R-loop locking, which occurs when the R-loop approaches the protospacer end, is the actual signal for Cas3 recruitment and whether protospacer mutations would interfere with this process. Our supercoiling experiments allow precise control over the formation of a locked R-loop, such that we can unambiguously distinguish whether the failure to cleave a mutant target would be due to the absence of R-loop formation, absence of R-loop locking, or failure of Cas3 recruitment.

We first established DNA cleavage experiments for a WT protospacer by monitoring up to 29 DNA molecules in parallel (Ramanathan et al., 2009). We identified nicked and supercoilable molecules, added 0.5 nM Cascade, and verified R-loop formation for the supercoilable molecules. We kept the molecules at F = 0.3 pN and −8 turns, added 100 nM Cas3, and monitored DNA nicking and cleavage (Figure 4A). Nicking was observed as an abrupt DNA length increase up to the length of

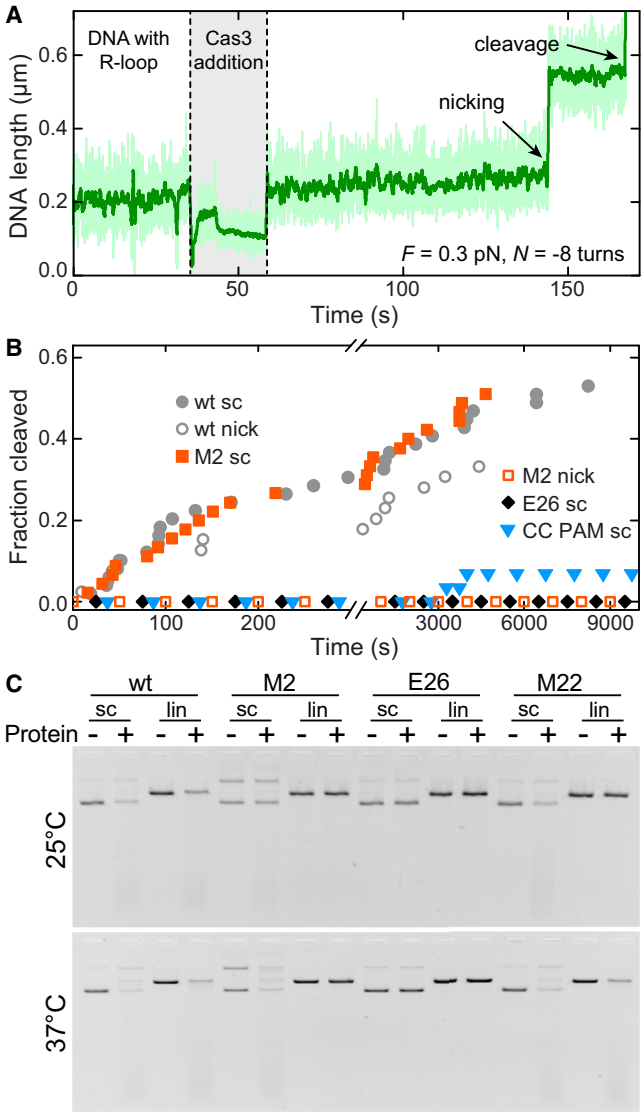

Figure 4. Cas3-Mediated DNA Cleavage of Preformed R-Loops

(A) Time trajectory of the DNA length for a single DNA-cleavage event. Supercoilable DNA with an R-loop on a WT protospacer was maintained at −8 turns. Following addition of Cas3 by buffer flow, DNA nicking and cleavage can be seen as a length increase and a subsequent loss of magnetic bead tracking, respectively. For the supercoilable molecules, DNA cleavage (n = 51) was preceded by a distinct nicking event in 73% of the cases.

(B) Fraction of DNA molecules cleaved as function of time for WT, M2, and E26 protospacers and a WT protospacer with a CC PAM. The data were separately obtained for the supercoilable molecules, for which R-loops were introduced in a controllable manner (filled symbols), and non-supercoilable molecules, where R-loop formation is not supported by induced torque (open symbols).

(C) Cleavage of supercoiled and linearized plasmid DNA containing either WT, M2, M22, or E26 protospacers analyzed by agarose gel experiments. Reactions were incubated for 40 min. More-detailed cleavage kinetics are shown in Figure S3.

non-supercoiled DNA, whereas cleavage was seen as loss of the magnetic bead. Of all supercoilable molecules (n = 49), 53% were cleaved and 4% were only nicked within ~2 hr (Figure 4B). The cleavage kinetics could be described with a double exponential, with 57% of events occurring with a time constant of 110 ± 20 s and the remaining with a time constant of ~4,000 s. Cleavage was also observed on 41% of all non-supercoilable molecules (i.e., molecules with poor surface attachment or randomly positioned nicks; n = 39). R-loops apparently also formed in this case, in agreement with the low negative torque required for the WT protospacer, albeit at a little lower efficiency, because the fraction of molecules with fast cleavage was only 35%.

We next tested DNA cleavage of the M2 protospacer that strongly inhibits R-loop formation (Figure 2A) and phage/plasmid interference (Semenova et al., 2011; Fineran et al., 2014). For the supercoilable molecules, we introduced R-loops at high negative torque and verified their presence before adding Cas3 under the same conditions as for the WT protospacer. We obtained a similar efficiency of cleavage (56%; n = 45) and cleavage rate (55% of cleavage occurring with a time constant of 130 ± 20 s; Figure 4B). However, for the non-supercoilable M2 molecules, cleavage was never observed (n = 16). This is in agreement with the requirement for an assisting negative torque to drive R-loop formation on the M2 protospacer; such torque is not possible with non-supercoilable DNA. The rapid cleavage of preformed R-loops on an M2 protospacer suggests that locking is the only requirement for Cas3 recruitment and that there is no further proofreading of the heteroduplex after locking.

To further substantiate the importance of the locking step, we investigated DNA cleavage of the E26 protospacer for which 25-bp R-loops are formed at negative supercoiling but for which locking is not observed (Szczelkun et al., 2014). When keeping such R-loops stabilized by the application of negative torque and adding Cas3, cleavage did not occur (n = 49; Figure 4B). Likewise, non-supercoilable molecules were never cleaved (n = 12). This further supports that R-loop locking is the only prerequisite for triggering the cleavage reaction.

To investigate the role of the PAM during cleavage triggering, we induced R-loops on a WT protospacer with a non-permissive CC-PAM (Sinkunas et al., 2013) using extensive negative supercoiling (−80 turns; 2.5 pN; ~30 min waiting time). R-loops formed on this substrate with moderate efficiency (Szczelkun et al., 2014). Importantly, only 7% of the supercoilable, R-loop-containing molecules were cleaved after ~1 hr when Cas3 was added (n = 29; Figure 4B), suggesting that PAM verification is also important for the cleavage step.

In a more physiologically relevant setting, we investigated Cas3-mediated cleavage of supercoiled and linearized plasmid DNA (Figures 4C and S3). Both DNA species were cleaved for the WT protospacer. Neither species was cleaved for protospacer E26. Protospacers M2 and M22 were cleaved in supercoiled plasmids, but not in the linearized form at 25°C. At 37°C, minor DNA degradation was observed for linearized M22 plasmids. These observations are in full agreement with the single-molecule results and supports the idea that the torque provided by negative supercoiling of plasmid DNA and/or the DNA melting afforded by elevating the temperature assist R-loop formation, in particular on mutated protospacers. On all DNA, once the locking step occurs, the DNA is destined to be cleaved.

DISCUSSION

R-Loops in *St*-Cascade Form Unidirectionally, Starting from the PAM

Directional R-loop propagation that is initiated at the PAM and further extends toward the protospacer end has been a long-standing hypothesis for DNA targeting by CRISPR-Cas systems (Semenova et al., 2011). Such a mechanism was corroborated by position-dependent effects of protospacer mutations on effector complex binding (Sternberg et al., 2014). In addition, we previously demonstrated differential effects of mutations near the two protospacer ends (Szczelkun et al., 2014). Whereas PAM mutations exclusively inhibited R-loop formation, mutations at the PAM distal protospacer end exclusively affected the R-loop stability. The results obtained so far are clearly in agreement with a directional R-loop formation model but could also be explained by a direction-independent mechanism (see Introduction). Using single-molecule supercoiling experiments, we provide here compelling evidence for a directional R-loop zipping. In particular, we were able to measure with close to base-pair resolution the length of R-loop intermediates that form on protospacers carrying single mismatches between the target sequence and the crRNA guide. Strikingly, the length of the R-loop intermediate corresponded directly to the distance between the PAM and the first mismatch. Other intermediates—e.g., corresponding to an R-loop behind the PAM—were not observed, which indicates a stringent unidirectional process. R-loops intermediates as short as 7 bp could be detected (see M8 data in Figure 2B). However, as the length of the intermediate shortened, the rate of spontaneous dissociation increased, even at significant negative supercoiling levels (Figure 3). Single 7-bp-long intermediates were too short-lived to be detected (though the intermediate state was occupied at higher Cascade concentrations), and we speculate that intermediates for M2 and M4 are so short lived that the intermediate state is rarely populated, even at higher Cascade concentrations. Accordingly, these protospacers were better competitors than a non-specific protospacer. R-loop intermediates were not detected for M19 in agreement with protein-induced base flips in the crRNA-DNA hybrid being at locations 7, 13, 19, 25, and 31 for *St*-Cascade.

Collapse of Short R-Loop Intermediates Ensures Efficient Target Localization

For the protospacers with single mutations, the R-loop formation kinetics were reduced (most severely for seed mutations), whereas the R-loop stability at positive torque was not affected. This kinetic inhibition of R-loop formation at unaltered R-loop stability is very similar to observations with PAM mutants (Szczelkun et al., 2014). Given that the PAM-recognizing motifs in Cas9 assist only in flipping of the first protospacer base toward the crRNA (Anders et al., 2014), we suggest a similar local priming at the PAM for Cascade. Priming at a permissive PAM is either promoted through conformational changes of the protein complex upon PAM binding or simply through a longer residence time at the PAM.

Upon priming, R-loop expansion is initiated. As discussed above, this R-loop can collapse in a length-dependent manner upon encountering mismatch sites. Consequently, the Cascade complex would be expected to have a shorter residence time on DNA with PAM-proximal mutations compared to DNA with PAM-distal mutations. This was additionally supported by competition experiments that revealed that the targets with seed mutations are much poorer competitors than targets with PAM-distal mutations (Figure 3C). The correlation between directional zipping and stability provides an efficient target site search process, by only considering targets with sufficient homology directly at the start of the process and rejecting all others. Similar proofreading by directional zipping may be employed in other biological processes where homologous sequences need to be found, such as homologous recombination, where a wealth of off targets need to be discriminated (De Vlaminck et al., 2012). Crucial features of an efficient search process would be that the off-target rejection is dependent on the length of the base-paired intermediate and that early mutations have a greater effect, as suggested by the wide-spread occurrence of seed sequences in other biological systems (Künne et al., 2014). Whereas here we provide evidence for such a length dependence, it remains yet to be established to which extent protein contacts contribute to the off-target rejection by Cascade.

Directional, Collapse-Prone R-Loop Zipping Is the Only Target Recognition Mechanism

The formation of an R-loop is not per se the signal for Cas3-mediated DNA cleavage. To trigger cleavage, the R-loop has to reach the protospacer end and become locked (i.e., highly resistant to positive supercoiling). Locking occurs only for R-loops that extend beyond position 28 (Szczelkun et al., 2014). For unlocked R-loops (E26 protospacer), cleavage did not occur at all (Figure 4). In contrast, an R-loop that was locked but contained a mismatch in the seed region promoted cleavage with a rate similar to the WT protospacer. This suggests that the Cascade-crRNA-promoted target recognition and the Cas3-mediated DNA cleavage steps are fully separated, i.e., that mismatches between DNA target and crRNA have no effect on the catalytic activity of Cas3. Thus, the directional, collapse-prone R-loop zipping represents the only target-verification mechanism.

Previous investigation showed that cleavage requires dsDNA at the PAM (Hochstrasser et al., 2014). Here, we additionally show that also the PAM sequence is verified during the actual cleavage step, because cleavage of locked R-loops is significantly reduced for a CC-PAM substrate (Figure 4B). Thus, Cascade simultaneously checks both ends of the protospacer, namely the PAM and the lock, before triggering cleavage. It needs to be further explored whether the additional PAM verification controls Cas3 recruitment or whether it promotes a conformational change that brings pre-bound Cas3 into a cleavage-competent state. The double checking of the PAM sequence may be required to avoid degradation of ssDNA intermediates (e.g., formed during DNA replication), which may bind to the crRNA and induce locking. Overall, the lack of protospacer proof-reading during the cleavage step in type I systems represents a significant difference to Cas9 of type II systems (Szczelkun et al., 2014; Cencic et al., 2014). Cas9 lacks an R-loop locking to verify complete R-loop formation (Szczelkun et al., 2014) and must thus also proof-read the target during the cleavage step.

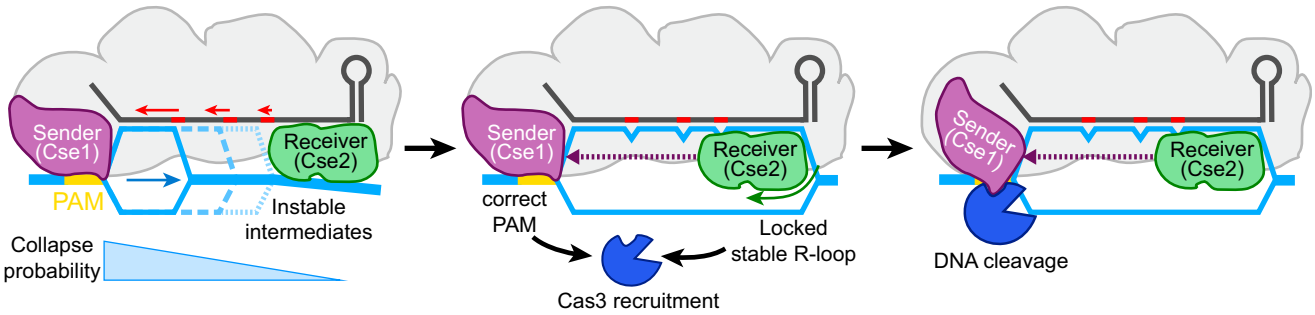

Figure 5. Model for Target Recognition and Off-Target Rejection by Cascade

Bidirectional telecommunication model for target recognition by Cascade, where an R-loop propagation is the only probe that verifies a potential target (left). When the R-loop reaches the protospacer end, it becomes locked. Locking and additional PAM verification at the other end (middle) trigger cleavage without additional proofreading for mismatches between crRNA and DNA (right). Note that the conformational changes including locking as well as Cse2 and Cse1 repositioning are considered to be part of a global allosteric mechanism. See text for details.

A Bidirectional "Telecommunication" Model for Target Recognition and Cleavage by Cascade

How can readout of distal signals—the PAM and the locking step—result in Cas3 recruitment and signaling of cleavage? We propose a bidirectional telecommunication model that relies on allostery for the target site discrimination by Cascade (see Figure 5). In this model, R-loop propagation serves as the only verification of a potential target and is key to rejection of off-target sites. R-loops become primed at the PAM through the Cse1 subunit, which acts as an R-loop "sender." Initiation is assisted by negative supercoiling, and R-loops propagate directionally away from the PAM. If a mismatch occurs, R-loop progression stalls. The R-loop intermediates collapse in a length-dependent manner, ensuring lower residence times at targets with mismatches closer to the PAM. However, R-loop progression can bypass a mismatch and continue to the protospacer end. Due to a steric clash (Mulepati et al., 2014), the arriving R-loop causes the Cse2 dimer to move, such that conformational signals are passed back toward the PAM. This conformational change is most likely a large allosteric conformational rearrangement of the whole complex. It also provides the locking of the R-loop (Szczelkun et al., 2014) by Cse2 contacts with the flipped-out bases of the target DNA and possibly also with the non-target DNA (Mulepati et al., 2014). Dependent on an additional PAM verification, but without further target proofreading, the allosteric coupling induces a rearrangement of Cse1, leading to recruitment of Cas3 near the PAM proximal site of the protospacer (Hochstrasser et al., 2014; Huo et al., 2014) and subsequent DNA degradation (Sinkunas et al., 2013). Within this model, we propose that mainly the repositioning of the Cse2 dimer establishes the R-loop locking. Further studies are required to directly demonstrate the conformational coupling and dynamics of the Cascade subunits during R-loop priming, locking, and Cas3 recruitment.

Overall, our study shows that target recognition and off-target rejection by Cascade relies just on a directional zipping and the collapse of semi-stable R-loop intermediates. We suggest that other DNA-targeting CRISPR-Cas surveillance complexes, among them Cas9, also use the same R-loop-formation mechanism. A careful consideration of the details of the R-loop-zipping process, together with a more-detailed analysis of the energetic barriers imposed by mismatches, opens the door to develop quantitative predictors for off-target cleavage. This should enable a more rational design of potential target sequences within large genomes to further minimize off-target cleavage events.

EXPERIMENTAL PROCEDURES

DNA and Proteins

Cascade with crRNA that matches spacer 1 of the *St*-CRISPR4 system was purified as described (Sinkunas et al., 2013). DNA substrates contained a WT protospacer that was fully complementary to spacer 1 or protospacer variants (Table S1) and an AA dinucleotide PAM (Figure 1A), except for a cleavage experiment where a WT protospacer with a CC PAM was used (Figure 4B). DNA constructs used in the tweezers experiments were prepared as previously described (Szczelkun et al., 2014). A single copy of a given protospacer was cloned into the SmaI site of plasmid pUC19. A 2.1-kbp fragment containing the protospacer and terminal NotI and SpeI restriction enzyme sites was amplified from the plasmid by PCR and ligated to ~600-bp PCR fragments containing multiple biotins and a single sticky end complementary to SpeI as well as ~600-bp PCR fragments containing multiple digoxigenins and a single sticky end complementary to NotI.

Single-Molecule Experiments

R-loop-formation experiments were carried out in 20 mM Tris-HCl (pH 8.0), 150 mM NaCl, and 0.1 mg ml^{-1} BSA at 9 nM or 0.1 nM Cascade using a home-built magnetic tweezers setup (Klaue and Seidel, 2009). DNA molecules were bound to 1 μm magnetic beads (MyOne; Invitrogen) and anchored in the flow cells (Luzzietti et al., 2012; Schwarz et al., 2013). After lowering the magnets to stretch tethered molecules, DNA length measurements were started. Data were recorded at an acquisition frequency of 120 Hz (shown in light gray or light blue in time trajectory plots) and smoothed to 2 Hz using a sliding average filter (dark colors in all DNA length plots). After initial DNA characterization, proteins were added and changes in DNA length observed as a function of applied force and DNA turns. Torque values were calculated based on previous theoretical work (Maffeo et al., 2010; Schöpflin et al., 2012; see also Supplemental Information). Home-written software used for these calculations is available for download at the author's website: http://www.uni-muenster.de/Biologie.AllgmZoo/Gruppen/Seidel/Download.

Cas3 cleavage experiments were carried out by preassembling R-loops on single DNA molecules at negative supercoiling using 0.5 nM Cascade (9 nM for the WT protospacer with a CC PAM) in a cleavage buffer (10 mM Tris-HCl [pH 7.5], 75 mM NaCl, 40 mM KCl, 7% [v/v] glycerol, 1.5 mM $MgCl_2$, 0.1 mM $NiCl_2$, 2 mM ATP, and 0.1 mg ml^{-1} BSA). After verifying R-loop formation, 100 nM Cas3 in cleavage buffer was added.

Mean R-loop formation and dissociation times were determined from exponential fits to cumulative distributions of the data (Szczelkun et al., 2014). Each mean-time value was calculated from ~25 events. Supercoiling changes were analyzed as described before (Szczelkun et al., 2014). They were either obtained from sudden height changes divided by the slope of the supercoiling curves at the given force (Figures 2B, right, and 3B) or from the shift of one of the sides of the supercoiling curve (Figure 2B).

Inhibition Experiments

Synthetic oligoduplexes (Sigma) bearing an AA PAM and a WT protospacer were labeled at the 5′ end using T4 polynucleotide kinase (Thermo Scientific) and [γ^{33}P]ATP (Hartmann Analytic). Increasing concentrations of unlabeled competitor oligoduplexes containing protospacers with mutations were mixed with 1 nM of labeled oligoduplexes and incubated with 10 nM of Cascade in binding buffer (40 mM Tris, 20 mM acetic acid, 1 mM EDTA [pH 8.0], 150 mM NaCl, 0.1 mg ml^{-1} BSA, and 10% glycerol) for 30 min at 37°C. The samples were subjected to electrophoresis in 8% (w/v) polyacrylamide gel and visualized using a FLA-5100 phosphorimager (Fujifilm). The fraction of Cascade-bound labeled DNA as function of competitor concentration was fitted with an expression that describes competitive inhibition in order to obtain the ratio K_I/K_D between the dissociation constants of competitor and substrate binding to Cascade (see Supplemental Information).

Bulk DNA Cleavage Experiments

Cleavage reactions were performed at 25°C and 37°C for 40 min in buffer containing 10 mM Tris-HCl (pH 8), 100 mM NaCl, 50 mM KCl, 5% (v/v) glycerol, 1.5 mM $MgCl_2$, 0.1 mM $NiCl_2$, 2 mM ATP, and 0.1 mg/ml BSA. Cleavage of 2.5 nM supercoiled or BamHI-linearized protospacer-containing plasmids was initiated by addition of 20 nM Cascade and 100 nM Cas3. Reactions were stopped by adding 1/3 of "Stop" solution (67.5 mM EDTA, 27% [v/v] glycerol, and 0.3% [w/v] SDS). Reaction products were analyzed by 0.8% (w/v) agarose gel electrophoresis and visualized by ethidium bromide staining.

SUPPLEMENTAL INFORMATION

Supplemental Information includes Supplemental Experimental Procedures, three figures, and one table and can be found with this article online at http://dx.doi.org/10.1016/j.celrep.2015.01.067.

AUTHOR CONTRIBUTIONS

V.S. and R.S. designed research. M.R., I.S., T.S., and M.S.T. performed research. V.S. and R.S. wrote the paper. All authors contributed to data analysis.

ACKNOWLEDGMENTS

We thank Ina Kowsky and Gerda Scheidgen-Kleyboldt for the preparation of DNA constructs, Giedrius Sasnauskas for discussions, and Christophe Rouillon and Mark Szczelkun for comments on the manuscript. This work was supported by a starting grant of the European Research Council (261224) to R.S. and the European Social Fund under Global Grant Measure Grant R100 to V.S. I.S. was supported by a scholarship from World Federation of Scientists.

Received: November 27, 2014
Revised: January 9, 2015
Accepted: January 28, 2015
Published: March 5, 2015

REFERENCES

Anders, C., Niewoehner, O., Duerst, A., and Jinek, M. (2014). Structural basis of PAM-dependent target DNA recognition by the Cas9 endonuclease. Nature *513*, 569–573.

Barrangou, R., Fremaux, C., Deveau, H., Richards, M., Boyaval, P., Moineau, S., Romero, D.A., and Horvath, P. (2007). CRISPR provides acquired resistance against viruses in prokaryotes. Science *315*, 1709–1712.

Brouns, S.J.J., Jore, M.M., Lundgren, M., Westra, E.R., Slijkhuis, R.J.H., Snijders, A.P.L., Dickman, M.J., Makarova, K.S., Koonin, E.V., and van der Oost, J. (2008). Small CRISPR RNAs guide antiviral defense in prokaryotes. Science *321*, 960–964.

Brutzer, H., Luzzietti, N., Klaue, D., and Seidel, R. (2010). Energetics at the DNA supercoiling transition. Biophys. J. *98*, 1267–1276.

Carte, J., Wang, R., Li, H., Terns, R.M., and Terns, M.P. (2008). Cas6 is an endoribonuclease that generates guide RNAs for invader defense in prokaryotes. Genes Dev. *22*, 3489–3496.

Cencic, R., Miura, H., Malina, A., Robert, F., Ethier, S., Schmeing, T.M., Dostie, J., and Pelletier, J. (2014). Protospacer adjacent motif (PAM)-distal sequences engage CRISPR Cas9 DNA target cleavage. PLoS ONE *9*, e109213.

De Vlaminck, I., van Loenhout, M.T.J., Zweifel, L., den Blanken, J., Hooning, K., Hage, S., Kerssemakers, J., and Dekker, C. (2012). Mechanism of homology recognition in DNA recombination from dual-molecule experiments. Mol. Cell *46*, 616–624.

Deveau, H., Barrangou, R., Garneau, J.E., Labonté, J., Fremaux, C., Boyaval, P., Romero, D.A., Horvath, P., and Moineau, S. (2008). Phage response to CRISPR-encoded resistance in Streptococcus thermophilus. J. Bacteriol. *190*, 1390–1400.

Fineran, P.C., Gerritzen, M.J.H., Suárez-Diez, M., Künne, T., Boekhorst, J., van Hijum, S.A.F.T., Staals, R.H.J., and Brouns, S.J.J. (2014). Degenerate target sites mediate rapid primed CRISPR adaptation. Proc. Natl. Acad. Sci. USA *111*, E1629–E1638.

Forth, S., Deufel, C., Sheinin, M.Y., Daniels, B., Sethna, J.P., and Wang, M.D. (2008). Abrupt buckling transition observed during the plectoneme formation of individual DNA molecules. Phys. Rev. Lett. *100*, 148301.

Gasiunas, G., Barrangou, R., Horvath, P., and Siksnys, V. (2012). Cas9-crRNA ribonucleoprotein complex mediates specific DNA cleavage for adaptive immunity in bacteria. Proc. Natl. Acad. Sci. USA *109*, E2579–E2586.

Hochstrasser, M.L., Taylor, D.W., Bhat, P., Guegler, C.K., Sternberg, S.H., Nogales, E., and Doudna, J.A. (2014). CasA mediates Cas3-catalyzed target degradation during CRISPR RNA-guided interference. Proc. Natl. Acad. Sci. USA *111*, 6618–6623.

Howan, K., Smith, A.J., Westblade, L.F., Joly, N., Grange, W., Zorman, S., Darst, S.A., Savery, N.J., and Strick, T.R. (2012). Initiation of transcription-coupled repair characterized at single-molecule resolution. Nature *490*, 431–434.

Huhle, A., Klaue, D., Brutzer, H., Daldrop, P., Joo, S., Otto, O., Keyser, U.F., and Seidel, R. (2015). Camera-based three-dimensional real-time particle tracking at kHz rates and Ångström accuracy. Nat. Commun. *6*, 5885.

Huo, Y., Nam, K.H., Ding, F., Lee, H., Wu, L., Xiao, Y., Farchione, M.D., Jr., Zhou, S., Rajashankar, K., Kurinov, I., et al. (2014). Structures of CRISPR Cas3 offer mechanistic insights into Cascade-activated DNA unwinding and degradation. Nat. Struct. Mol. Biol. *21*, 771–777.

Jackson, R.N., Golden, S.M., van Erp, P.B.G., Carter, J., Westra, E.R., Brouns, S.J.J., van der Oost, J., Terwilliger, T.C., Read, R.J., and Wiedenheft, B. (2014). Structural biology. Crystal structure of the CRISPR RNA-guided surveillance complex from Escherichia coli. Science *345*, 1473–1479.

Kauert, D.J., Kurth, T., Liedl, T., and Seidel, R. (2011). Direct mechanical measurements reveal the material properties of three-dimensional DNA origami. Nano Lett. *11*, 5558–5563.

Klaue, D., and Seidel, R. (2009). Torsional stiffness of single superparamagnetic microspheres in an external magnetic field. Phys. Rev. Lett. *102*, 028302.

Künne, T., Swarts, D.C., and Brouns, S.J.J. (2014). Planting the seed: target recognition of short guide RNAs. Trends Microbiol. *22*, 74–83.

Luzzietti, N., Knappe, S., Richter, I., and Seidel, R. (2012). Nicking enzyme-based internal labeling of DNA at multiple loci. Nat. Protoc. *7*, 643–653.

Maffeo, C., Schöpflin, R., Brutzer, H., Stehr, R., Aksimentiev, A., Wedemann, G., and Seidel, R. (2010). DNA-DNA interactions in tight supercoils are described by a small effective charge density. Phys. Rev. Lett. *105*, 158101.

Mali, P., Yang, L., Esvelt, K.M., Aach, J., Guell, M., DiCarlo, J.E., Norville, J.E., and Church, G.M. (2013). RNA-guided human genome engineering via Cas9. Science *339*, 823–826.

Mosconi, F., Allemand, J.F., Bensimon, D., and Croquette, V. (2009). Measurement of the torque on a single stretched and twisted DNA using magnetic tweezers. Phys. Rev. Lett. *102*, 078301.

Mulepati, S., and Bailey, S. (2013). In vitro reconstitution of an Escherichia coli RNA-guided immune system reveals unidirectional, ATP-dependent degradation of DNA target. J. Biol. Chem. *288*, 22184–22192.

Mulepati, S., Héroux, A., and Bailey, S. (2014). Structural biology. Crystal structure of a CRISPR RNA-guided surveillance complex bound to a ssDNA target. Science *345*, 1479–1484.

Oberstrass, F.C., Fernandes, L.E., and Bryant, Z. (2012). Torque measurements reveal sequence-specific cooperative transitions in supercoiled DNA. Proc. Natl. Acad. Sci. USA *109*, 6106–6111.

Otto, O., Czerwinski, F., Gornall, J.L., Stober, G., Oddershede, L.B., Seidel, R., and Keyser, U.F. (2010). Real-time particle tracking at 10,000 fps using optical fiber illumination. Opt. Express *18*, 22722–22733.

Ramanathan, S.P., van Aelst, K., Sears, A., Peakman, L.J., Diffin, F.M., Szczelkun, M.D., and Seidel, R. (2009). Type III restriction enzymes communicate in 1D without looping between their target sites. Proc. Natl. Acad. Sci. USA *106*, 1748–1753.

Schöpflin, R., Brutzer, H., Müller, O., Seidel, R., and Wedemann, G. (2012). Probing the elasticity of DNA on short length scales by modeling supercoiling under tension. Biophys. J. *103*, 323–330.

Schwarz, F.W., Tóth, J., van Aelst, K., Cui, G., Clausing, S., Szczelkun, M.D., and Seidel, R. (2013). The helicase-like domains of type III restriction enzymes trigger long-range diffusion along DNA. Science *340*, 353–356.

Semenova, E., Jore, M.M., Datsenko, K.A., Semenova, A., Westra, E.R., Wanner, B., van der Oost, J., Brouns, S.J.J., and Severinov, K. (2011). Interference by clustered regularly interspaced short palindromic repeat (CRISPR) RNA is governed by a seed sequence. Proc. Natl. Acad. Sci. USA *108*, 10098–10103.

Sinkunas, T., Gasiunas, G., Fremaux, C., Barrangou, R., Horvath, P., and Siksnys, V. (2011). Cas3 is a single-stranded DNA nuclease and ATP-dependent helicase in the CRISPR/Cas immune system. EMBO J. *30*, 1335–1342.

Sinkunas, T., Gasiunas, G., Waghmare, S.P., Dickman, M.J., Barrangou, R., Horvath, P., and Siksnys, V. (2013). In vitro reconstitution of Cascade-mediated CRISPR immunity in Streptococcus thermophilus. EMBO J. *32*, 385–394.

Sternberg, S.H., Redding, S., Jinek, M., Greene, E.C., and Doudna, J.A. (2014). DNA interrogation by the CRISPR RNA-guided endonuclease Cas9. Nature *507*, 62–67.

Szczelkun, M.D., Tikhomirova, M.S., Sinkunas, T., Gasiunas, G., Karvelis, T., Pschera, P., Siksnys, V., and Seidel, R. (2014). Direct observation of R-loop formation by single RNA-guided Cas9 and Cascade effector complexes. Proc. Natl. Acad. Sci. USA *111*, 9798–9803.

Tamulaitis, G., Kazlauskiene, M., Manakova, E., Venclovas, Č., Nwokeoji, A.O., Dickman, M.J., Horvath, P., and Siksnys, V. (2014). Programmable RNA shredding by the type III-A CRISPR-Cas system of Streptococcus thermophilus. Mol. Cell *56*, 506–517.

Westra, E.R., van Erp, P.B.G., Künne, T., Wong, S.P., Staals, R.H.J., Seegers, C.L.C., Bollen, S., Jore, M.M., Semenova, E., Severinov, K., et al. (2012). CRISPR immunity relies on the consecutive binding and degradation of negatively supercoiled invader DNA by Cascade and Cas3. Mol. Cell *46*, 595–605.

Zhang, J., Rouillon, C., Kerou, M., Reeks, J., Brugger, K., Graham, S., Reimann, J., Cannone, G., Liu, H., Albers, S.-V., et al. (2012). Structure and mechanism of the CMR complex for CRISPR-mediated antiviral immunity. Mol. Cell *45*, 303–313.

Zhao, H., Sheng, G., Wang, J., Wang, M., Bunkoczi, G., Gong, W., Wei, Z., and Wang, Y. (2014). Crystal structure of the RNA-guided immune surveillance Cascade complex in Escherichia coli. Nature *515*, 147–150.